This article has been accepted for publication in a future issue of this journal, but has not been fully edited. Content may change prior to final publication. Citation information: DOI 10.1109/LMWC.2021.3066282, IEEE Microwave and Wireless Components Letters



# 3–20 GHz GaN MMIC Power Amplifier Design Through a $C_{\mathrm{OUT}}$ Compensation Strategy

Jorge Julian Moreno Rubio, Roberto Quaglia, *Member, IEEE*, Anna Piacibello, *Member, IEEE*, Vittorio Camarchia, *Senior Member, IEEE*, Paul J. Tasker, *Fellow, IEEE* and Steve Cripps, *Life Fellow, IEEE*

***Abstract*—This paper presents the design approach for a compact, single-stage, wideband MMIC power amplifier. A method is proposed to compensate the output capacitance of the active device over a frequency range as wide as possible, with minimum impact on the achievable output power, that leads to a 2-element compensating network. A 3-section transformer is then adopted for a real-to-real transformation. The CW characterization shows output power higher than 32 dBm and drain efficiency between 35% and 45%, over a fractional bandwidth of 148%, from 3 GHz to 20 GHz.**

***Index Terms*—Broadband matching networks, FETs, GaN, Microwave amplifiers, Wideband.**

## I. Introduction

Future high performance broadband systems, such as RF and microwave front-end systems, radar and software reconfigurable communication links, require wideband Microwave Monolithic Integrated Circuit (MMIC) power amplifiers (PAs). Gallium Nitride (GaN) High Electron Mobility Transistors (HEMTs) are becoming the technology of choice for the PA thanks their high power density at microwaves frequencies. To achieve decade-bandwidth performance distributed PAs are typically used, normally in a non-uniform topology to improve output power and efficiency [1]–[4]. Other wideband GaN PAs have been proposed, relying for example on reactive matching [5] or on a reconfigurable dual-band operation [6], covering smaller bandwidths (6–18 GHz).

In this work, we propose a novel design strategy to compensate the output capacitance $C_{\mathrm{OUT}}$ of the HEMT for any device size, as long as $C_{\mathrm{OUT}}$ is an accurate representation of the output reactive effects of the device. A 3 – 20 GHz single-ended MMIC amplifier fabricated on a 100 nm GaN-on-Si process is presented to demonstrate the validity of the approach. The results compare well with the state of the art, see Table I, while relying on a simpler design approach, and using a single transistor and small MMIC area.

J. Moreno Rubio, R. Quaglia, P. J. Tasker and S. Cripps are with the Centre for High Frequency Engineering, Cardiff University, Queen's Buildings, The Parade, Cardiff CF24 3AA Wales, UK. e-mail: quagliar@cardiff.ac.uk

J. Moreno Rubio is also a member of the research group GINTEL, Universidad Pedagógica y Tecnológica de Colombia, Calle 4 Sur No. 15-134, Sogamoso, Colombia. e-mail: jorgejulian.moreno@uptc.edu.co

A. Piacibello and V. Camarchia are with with the Department of Electronics, Politecnico di Torino, 10129 Torino, Italy. e-mail: vittorio.camarchia@polito.it

A. Piacibello is also with the Microwave Engineering Center for Space Applications (MECSA), 00133 Rome, Italy.

## II. Design

### A. Optimal load identification

The optimal intrinsic load of a FET can be considered real and frequency-independent. However, the dispersion effects, which can be modelled with an equivalent output capacitance, make the extrinsic load strongly dependent on frequency. The PA design method proposed shows a specific, simple way of compensating $C_{\mathrm{OUT}}$, and then relies on a real-to-real transformation from the system impedance to the intrinsic optimum load.

In the estimation of the optimal extrinsic load, the device output capacitance $C_{\mathrm{OUT}}$ can be considered constant for the sake of simplicity [7], and it is estimated using Cold-FET simulations [8]. For the adopted device, a GaN-on-Si 100 nm gate-length $8 \times 100\,\mu$m device supplied by OMMIC, the obtained value for $C_{\mathrm{OUT}}$ is 0.37 pF.

As a reference, an idealized output network is shown in Fig. 1(b). The negative capacitance would compensate the effect of $C_{\mathrm{OUT}}$ at each frequency, and the resistor $R_{\mathrm{opt}}$ represents the optimal intrinsic load of the device. For this device, $R_{\mathrm{opt}} \approx 20\,\Omega$, taking into account a drain-to-source bias voltage: $V_{\mathrm{DD}} = 12\,\mathrm{V}$, knee voltage: $V_{\mathrm{k}} = 2\,\mathrm{V}$, Maximum current: $I_{\mathrm{M}} = 1\,\mathrm{A}$.

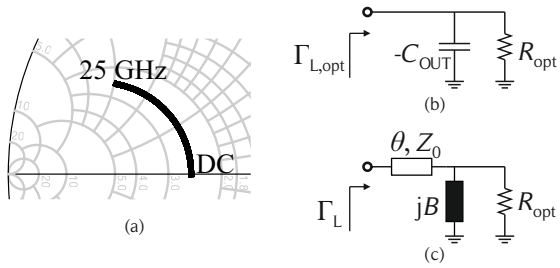


Fig. 1. Optimal load on the admittance Smith Chart (a), ideal OMN (b) and alternative OMN (c).

From Fig. 1(b), the optimal reflection coefficient $\Gamma_{\mathrm{opt}}$ is found to describe a constant conductance circle as a function of frequency, with centre in $-g_{\mathrm{opt}}/(1+g_{\mathrm{opt}})$ and radius $1/(1+g_{\mathrm{opt}})$, given by

$$\Gamma_{\mathrm{opt}} = -\frac{g_{\mathrm{opt}}}{1+g_{\mathrm{opt}}} + \frac{1}{1+g_{\mathrm{opt}}} e^{j2\arctan\left(\frac{2\pi f C_{\mathrm{OUT}} Z_0}{1+g_{\mathrm{opt}}}\right)} \quad (1)$$

where $Z_0$ is the reference impedance ($50\,\Omega$ in this case), $f$ is the frequency and $g_{\mathrm{opt}} = Z_0/R_{\mathrm{opt}}$. Fig. 1(a) illustrates the

This article has been accepted for publication in a future issue of this journal, but has not been fully edited. Content may change prior to final publication. Citation information: DOI 10.1109/LMWC.2021.3066282, IEEE Microwave and Wireless Components Letters



arc that represents $\Gamma_{\rm opt}$ over a set of frequencies from DC to 25 GHz, which is obtained using (1).

The resistance $R_{\rm opt} = 20\,\Omega$, in Fig. 1(b), can be synthesized from the reference system impedance $Z_0 = 50\,\Omega$, and with an arbitrary bandwidth, using a multi-section transformer. In other words, the required bandwidth can be guaranteed for this transformation by using enough sections for the transformer. It is important, however, to balance the number of sections between transformation accuracy and inserted losses and size. If this can be achieved reasonably in the technology adopted, then the problem reduces to designing a network, that synthesizes, as precisely as possible, the negative capacitance effect shown in Fig. 1(b).

### B. Idealized solution

In practice, the arc shown in Fig. 1(a) can not be synthesized by a single passive element. However, using a two-element network, an approximated solution can be found. In order to estimate the limitations of a practical solution, an idealized solution, which follows perfectly $\Gamma_{\rm opt}$ in (1), is studied. As illustrated in Fig. 1(c), it is composed of a shunt susceptance $B$ and a series transmission line of electrical length $\theta$ and characteristic impedance $Z_0$, where

$$B = \omega C_{\rm OUT} \tag{2}$$

and

$$\theta = \arctan\left(\frac{-2\,BY_0}{Y_0^2 - G_{\rm opt}^2 - B^2}\right) \tag{3}$$

with $\omega = 2\pi f$, $Y_0 = 1/Z_0$ and $G_{\rm opt} = 1/R_{\rm opt}$.

Equation (2) suggests that the most trivial implementation of the shunt susceptance is adopting a capacitor ($C_{\rm OUT}$). However, if $B$ is linearly dependent on frequency, from (3) it follows that the electrical length $\theta$ is not linear with frequency. This is a significant practical limitation, given the linear frequency dependence of the electrical length of transmission lines.

However, as a trade-off, an open stub can be used to synthesized $B$ instead of a capacitor. Thus, $B$ has a tangent-like dependence on frequency, which makes $\theta$ almost linear with frequency, as shown in the example of Fig. 2, and therefore better approximated by a common transmission line. Fig. 2 shows the frequency dependence of $\theta$ obtained using (3) for two cases, namely using the ideal capacitor solution for $B$ (2), and using an open stub.

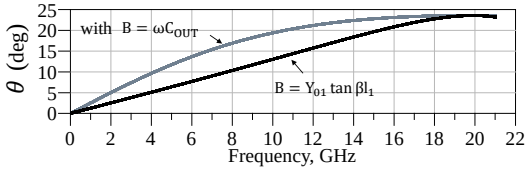


Fig. 2. Solution for (3) in two cases: $B$ synthesized by a capacitor (gray) and by an open stub (black).

### C. OMN design

Thus, assuming that $R_{\rm opt}$ is realized using a multi-section transformer, the proposed OMN is shown in Fig. 3(a). The reflection coefficient $\Gamma_{\rm L,p}$, obtained at the reference plane right after the stub, can then be expressed as

$$\Gamma_{\rm L,p} = -\frac{g_{\rm opt}}{1+g_{\rm opt}} + \frac{1}{1+g_{\rm opt}}\,e^{-j2\arctan\left(\frac{Z_0\tan\theta_1}{Z_{01}(1+g_{\rm opt})}\right)} \tag{4}$$

Eq. (4) represents an arc similar to (1) but mirrored with respect to the real axis of the Smith Chart, see Fig. 3(b). Adding a series transmission line in front of the stub, as illustrated in Fig. 3(b), the group of points represented by $\Gamma_{\rm L,p}$ turns clockwise on the Smith Chart, with an angle proportional to the frequency. Thus, assuming $Z_{02} = Z_0$, the expression for $\Gamma_{\rm L}$ in Fig. 3(a) is as follows:

$$\Gamma_{\rm L} = e^{-j2\,\theta_2}\Gamma_{\rm L,p}. \tag{5}$$

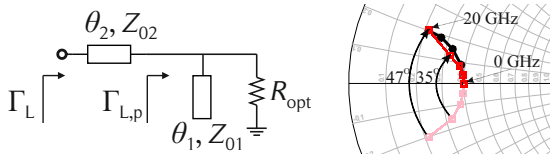


Fig. 3. Proposed OMN (a), and $\Gamma_{\rm L}$ obtained with open stub (red), $\Gamma_{\rm opt}$ (black) and $\Gamma_{\rm L,p}$ (pink) (b).

Using (5), a solution for $\theta_2$ and $\theta_1$ can be found, aiming to keep $\Gamma_{\rm L}$ close to $\Gamma_{\rm opt}$. In general, the value of $Z_{01}$ can be used as an optimization parameter to be selected before solving (5). In this case, for simplicity $Z_{01} = Z_{02} = Z_0 = 50\,\Omega$.

Since the condition $\Gamma_{\rm L}(0\,{\rm GHz}) = \Gamma_{\rm opt}(0\,{\rm GHz})$ is guaranteed according to our assumptions, and the susceptance is expected to decrease with frequency in both cases, a convenient solution for $\theta_2$ and $\theta_1$ can be obtained solving $\Gamma_{\rm L}(f_{\rm h}) = \Gamma_{\rm opt}(f_{\rm h})$, where $f_{\rm h}$ is a design parameter.

In order to select the value of $f_{\rm h}$, the magnitude of the intrinsic load impedance $Z_{\rm int} = 1/(Y_{\rm L} + j\,\omega C_{\rm OUT})$ can be observed over frequency. Thus, based on the bandwidth estimation method proposed in [9], the output power can be estimated, as follows

$$P_{\rm OUT} = \begin{cases} \frac{1}{8} I_{\rm M}^2 \Re\{Z_{\rm int}\}, & \text{if } f \le f_{\rm h} \\ \frac{1}{2}\left(V_{\rm DD} - V_{\rm k}\right)^2 \Re\{\frac{1}{Z_{\rm int}}\}, & \text{if } f > f_{\rm h} \end{cases} \tag{6}$$

The difference between the estimated saturated power $P_{\rm OUT}$ and the maximum expected power from the device assumed as $P_{\rm MAX} = 0.125\,I_{\rm M}^2\,R_{\rm opt} = 2.5\,{\rm W}$, for different choices of $f_{\rm h}$, is shown in Fig 4. In this case, targeting for a maximum power reduction over the band lower than 0.7 dB, $f_{\rm h}$ is selected to be 20 GHz, obtaining $\theta_2 = 23.6^o$ and $\theta_1 = 66.8^o$ at 20 GHz. Fig. 3(b) shows how the series transmission line produces different phase delays for different frequencies, and how in this way the synthesized reflection coefficient $\Gamma_{\rm L}$ can follow $\Gamma_{\rm opt}$ closely.

This article has been accepted for publication in a future issue of this journal, but has not been fully edited. Content may change prior to final publication. Citation information: DOI 10.1109/LMWC.2021.3066282, IEEE Microwave and Wireless Components Letters



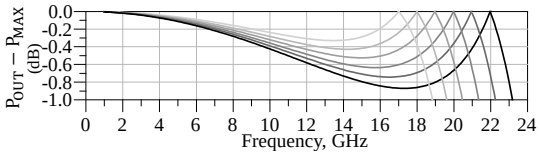


Fig. 4. Estimated output power for different values of $f_h$.

## III. Realization and Characterization

Fig. 5(a) illustrates the final schematic of the designed PA and its picture is shown in Fig. 5(b). The 20 Ω resistance is obtained through a 3-section Chebyshev transformer centered at 15.5 GHz. The open-circuited stub is finely tuned to compensate for the reactive effect of the high impedance bias-tee included in parallel. The series transmission line is implemented including a taper that fits with the device drain pin width. The load $\Gamma_{L,syn}$ synthesized by the OMN is compared to the theoretical one in Fig. 6, highlighting the good agreement between 5 GHz to 20 GHz. As expected the differences at the lowest frequencies are due to the the inclusion of the bias-tee and DC blocking capacitors.

The IMN has been designed to optimize the transducer gain over the band. A resistor has also been included for out- and in-band stabilization.

The scattering and CW characterization results over the band of interest are shown in Fig.7. On-wafer calibration at the probe tips has been used, while an extended coaxial port calibration has been adopted to enable the power calibration using a power meter. The achieved bandwidth is in line with the expected one, apart from a slight shift which affects the upper band edge. A saturated drain efficiency between 35% and 45% has been obtained over 17 GHz of bandwidth, from 3 GHz to 20 GHz. The corresponding PAE ranges from 27% to 38%, while the obtained saturated output power is higher than

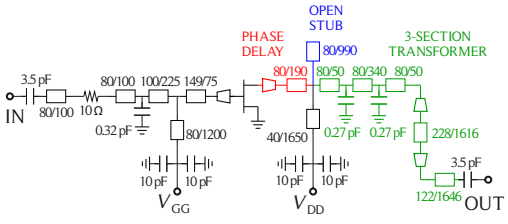


(a)

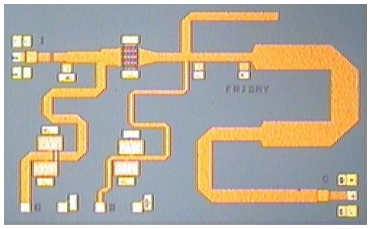

(b)

Fig. 5. Schematic (line dimensions are given as width/length in $\mu$m), device size: 8×100 $\mu$m, with 100 nm gate-length (a), and picture of the realized wideband PA (b). Chip size is 3 mm×2 mm

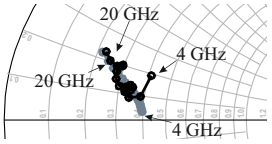


Fig. 6. Synthesized load $\Gamma_{L,syn}$ (black) and theoretical load $\Gamma_L$ (gray).

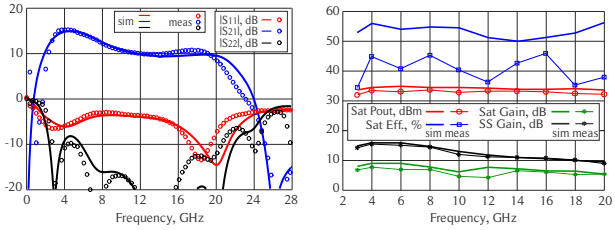


(a) (b)

Fig. 7. Comparison of simulated (solid) and measured (symbols): (a) $S_{1,1}$ (red), $S_{2,1}$ (blue) and $S_{2,2}$ (black), and (b) saturated output power (red), small signal gain (black), saturated gain (green) and saturated efficiency (blue).

32 dBm over the band, and the power gain is between 9 dB and 16 dB. Table I shows that the results are comparable to the state of the art, while using a simple design approach and a small size MMIC. The measured results are in rather good agreement with the simulations, except for the discrepancy in the saturated efficiency, which can be justified both by the CW measurements being carried out on wafer directly on a room temperature chuck, without dedicated die attachment, and by the fact that load pull measurements on the same device have shown the large signal model to overestimate both saturated power and efficiency [10].

TABLE I
State of the art of microwave GaN wideband power amplifiers.

| Ref. | Year | Area ($mm^2$) | BW (GHz) | BW (%) | Gain (dB) | $P_{OUT}$ (dBm) | PAE (%) |
|---|---|---|---|---|---|---|---|
| [1] | 2009 | 15 | 1.5–17 | 167 | 10–14 | >39.6 | 20–38 |
| [2] | 2011 | 38 | 2–20 | 165 | 9–15 | >40 | 15–36 |
| [3] | 2019 | 7.5 | 2–20 | 163 | 16–17.5 | >33.8 | 18–37 |
| [4] | 2019 | 7 | 2–18 | 160 | 28–30 | >39.6 | 18–38 |
| [5] | 2013 | 12 | 6–18 | 100 | 20–26 | >40 | 10–25 |
| [6] | 2018 | 5.1 | 6–18 | 100 | 15–27 | >34 | 15–34 |
| **This work** | **2020** | **6** | **3–20** | **148** | **9–16** | **>32** | **27–38** |

## IV. Conclusions

A compact multi-octave MMIC PA has been designed through a simple output capacitance compensation strategy. The obtained drain efficiency is shown to be between 35 % and 45 % over a 148 % fractional bandwidth, and with 32 dBm of output power, in line with state-of-the-art broadband PAs for RF and microwave front-end systems.

## Acknowledgment

This work was partially supported by the European Union's Horizon 2020 Research and Innovation Programme through the Marie Sklodowska-Curie agreement under grant 793529.

## REFERENCES


[1] C. Campbell, C. Lee, V. Williams, M. Kao, H. Tserng, P. Saunier, and T. Balisteri, "A Wideband Power Amplifier MMIC Utilizing GaN on SiC HEMT Technology," *IEEE Journal of Solid-State Circuits*, vol. 44, no. 10, pp. 2640–2647, 2009.

[2] J. J. Komiak, K. Chu, and P. C. Chao, "Decade bandwidth 2 to 20 GHz GaN HEMT power amplifier MMICs in DFP and No FP technology," in *2011 IEEE MTT-S International Microwave Symposium*, 2011, pp. 1–4.

[3] M. Roberg, S. Schafer, O. Marrufo, and T. Hon, "A 2–20 GHz Distributed GaN Power Amplifier Using a Novel Biasing Technique," in *2019 IEEE MTT-S International Microwave Symposium (IMS)*, 2019, pp. 694–697.

[4] H. Wu, Q. Lin, L. Zhu, S. Chen, Y. Chen, and L. Hu, "A 2 to 18 GHz Compact High-Gain and High-Power GaN Amplifier," in *2019 IEEE MTT-S International Microwave Symposium (IMS)*, 2019, pp. 710–713.

[5] U. Schmid, H. Sledzik, P. Schuh, J. Schroth, M. Oppermann, P. Brückner, F. van Raay, R. Quay, and M. Seelmann-Eggebert, "Ultra-Wideband GaN MMIC Chip Set and High Power Amplifier Module for Multi-Function Defense AESA Applications," *IEEE Trans. Microw. Theory Techn.*, vol. 61, no. 8, pp. 3043–3051, 2013.

[6] K. Choi, H. Park, M. Kim, J. Kim, and Y. Kwon, "A 6–18-GHz Switchless Reconfigurable Dual-Band Dual-Mode PA MMIC Using Coupled-Line-Based Diplexer," *IEEE Trans. Microw. Theory Techn.*, vol. 66, no. 12, pp. 5685–5695, 2018.

[7] J. J. Moreno Rubio, R. Quaglia, A. Baddeley, P. J. Tasker, and S. C. Cripps, "Design of a Broadband Power Amplifier Based on Power and Efficiency Contour Estimation," *IEEE Microw. Wireless Compon. Lett.*, pp. 1–3, 2020.

[8] Yeong-Lin Lai and Kuo-Hua Hsu, "A new pinched-off cold-FET method to determine parasitic capacitances of FET equivalent circuits," *IEEE Trans. Microw. Theory Techn.*, vol. 49, no. 8, pp. 1410–1418, 2001.

[9] J. J. Moreno Rubio, V. Camarchia, R. Quaglia, E. F. Angarita Malaver, and M. Pirola, "A 0.6 - 3.8 GHz GaN Power Amplifier Designed Through a Simple Strategy," *IEEE Microw. Wireless Compon. Lett.*, vol. 26, no. 6, pp. 446–448, June 2016.

[10] R. Quaglia, A. Piacibello, F. Costanzo, R. Giofrè, M. Casbon, R. Leblanc, V. Valenta, and V. Camarchia, "Source/Load-Pull Characterisation of GaN on Si HEMTs with Data Analysis Targeting Doherty Design," in *2020 IEEE Topical Conference on RF/Microwave Power Amplifiers for Radio and Wireless Applications (PAWR)*, 2020, pp. 5–8.